Triplet states of CO trapped in rare gas crystals

J. Bahrdt, P. Gürtler, and N. Schwentner

Citation: The Journal of Chemical Physics **86**, 6108 (1987); doi: 10.1063/1.452449
View online: http://dx.doi.org/10.1063/1.452449
View Table of Contents: http://scitation.aip.org/content/aip/journal/jcp/86/11?ver=pdfcov
Published by the AIP Publishing

Triplet states of CO trapped in rare gas crystals

J. Bahrdt, P. Gürtler,[a] and N. Schwentner
Institut für Atom- und Festkörperphysik, Freie Universität Berlin, Arnimallee 14, 1000 Berlin 33, Federal Republic of Germany

(Received 29 December 1986; accepted 20 February 1987)

Vibrational progressions due to the $a\,^3\Pi$, $a'\,^3\Sigma^+$, $d\,^3\Delta$, and $e\,^3\Sigma^-$ states of CO in Ar, Kr, and Xe crystals are observed in absorption. Two groups of phonon sidebands separated from the zero phonon lines by about 4 and 8 meV for the $a'\,^3\Sigma^+$ and $d\,^3\Delta$ states are attributed to librations and to localized phonons. The broad absorption bands, the even broader emission bands, and the large Stoke shift of the $a\,^3\Pi$ transition are treated in terms of a configuration coordinate model by a momentum analysis. A quadratic coupling has to be invoked with relaxation energies in the excited states increasing from 14 meV for Ar to 95 meV for Xe and with relaxation energies in the ground state increasing from 29 meV for Ar up to 1278 meV for Xe. The changes of the configuration coordinate of 0.2 to 1.5 Å are also discussed with the help of two pair potential models.

I. INTRODUCTION

The interaction of CO internal vibrations with librational modes and with localized and in-band lattice modes in rare gas matrices has been studied in the elctronic ground state.[1] The spin-allowed $A\,^1\Pi$ bands have been observed in several absorption experiments[2–4] and the line shapes have been discussed in terms of electron–phonon coupling.[2–4] The decay of the spin forbidden $a\,^3\Pi(v'=0)$ state to the ground state is the only transition reported in luminescence experiments.[5–8] Gas-to-matrix shifts have been related to site geometries including dispersive and inductive interactions of the CO guest with the rare gas host.[8] In this paper, absorption spectra of the $a\,^3\Pi(v') \leftarrow X\,^1\Sigma_g^+(v=0)$ vibrational progression, together with emission spectra, are presented for CO in Ar, Kr, and Xe crystals. With this information it is now possible to separate the Stokes shift due to electron–phonon coupling and the matrix shift for the ground state nuclear configuration. A comparison of the line shapes in absorption and emission will show that both linear coupling and quadratic coupling must be included in an analysis. A previous model[8] has to be revised. The interpretation of the data using the method of moments and a configuration coordinate model yields the relaxation energies in the ground and excited states and estimates of the dominant phonon modes coupling to the $X\,^1\Sigma_g^+$ and the $a\,^3\Pi$ states due to this electronic transition. Furthermore, highly resolved absorption spectra for the vibrational progression of all the other low-lying triplet states, $a'\,^3\Sigma^+$, $d\,^3\Delta$, and $e\,^3\Sigma^-$ will be presented which show zero phonon lines and several phonon sidebands. The gas to matrix shift, the electron–phonon coupling strength, and the local phonon modes coupling to these electronic transitions depend on the symmetry of the electronic states and on the matrices.

II. EXPERIMENTAL SETUP

These are the first experimental results taken at the high flux and high resolution 3 m NIM-2 beam line which is combined with a luminescence setup of high efficiency and is located at the storage ring BESSY in Berlin. Light emitted into 46 mrad of the horizontal and 4.4 mrad of the vertical emission cone of a BESSY bending magnet is focused by two mirrors, a cylindrical one (M1), and a plane–elliptical one (M2), at the entrance slit of a 3 m normal-incidence monochromator. The design (Fig. 1) is similar to that of SUPERLUMI at DORIS in Hamburg[9] but has been improved by ray-tracing calculations.[10] A focus size at the entrance slit of 2 mm horizontal and 0.15 mm vertical, limited by source size and aberrations, and a resolution of 0.005 nm with a 1200 lines/mm grating have been achieved. The light spot at the exit slit is imaged by a rotational–elliptic mirror in a 1:3 reduced scale onto the sample. The flux at the sample reaches 2×10^{13} photons $nm^{-1}\,s^{-1}$ for typical BESSY currents (Fig. 1). Luminescence radiation emitted by the sample is dispersed by two independent monochromators. Both use the focus on the sample as an entrance slit.

An $f/3.6$ Seya–Namioka monochromator with an ultimate resolution of 0.6 nm covers the vacuum ultraviolet range from 30 to 300 nm. The longer wavelength range (200 to 1000 nm) is recorded by an $f/3.8$ Ebert monochromator with a resolution of 0.5 nm. The light is detected by a fast channel-plate detector from Instrument Technology LTD for time-resolved studies using the standard time to amplitude conversion[11] or, in steady state experiments, by different photomultipliers (Valvo XP 2020 520, RCA C31034 A 102 GaAs, EMI G26H314 solar blind LF, Hamamatsu R 1460 solar blind).

Crystals of 1 cm^3 volume have been grown from gaseous mixtures of CO in Ar, Kr, or Xe with appropriate partial pressures in a Pyrex cell cooled by a closed cycle refrigerator to 15–20 K. Gases from Linde with a purity of 99.997%, 99.9999%, 99.998%, and 99.998% for CO, Ar, Kr, and Xe, respectively, have been used without further purification. The absorption and emission spectra showed no indication

[a] Present address: Deutsches Elektronen-Synchrotron DESY Notkestrasse 85, 2000 Hamburg 52, Federal Republic of Germany.

 0021-9606/87/116108-07$02.10

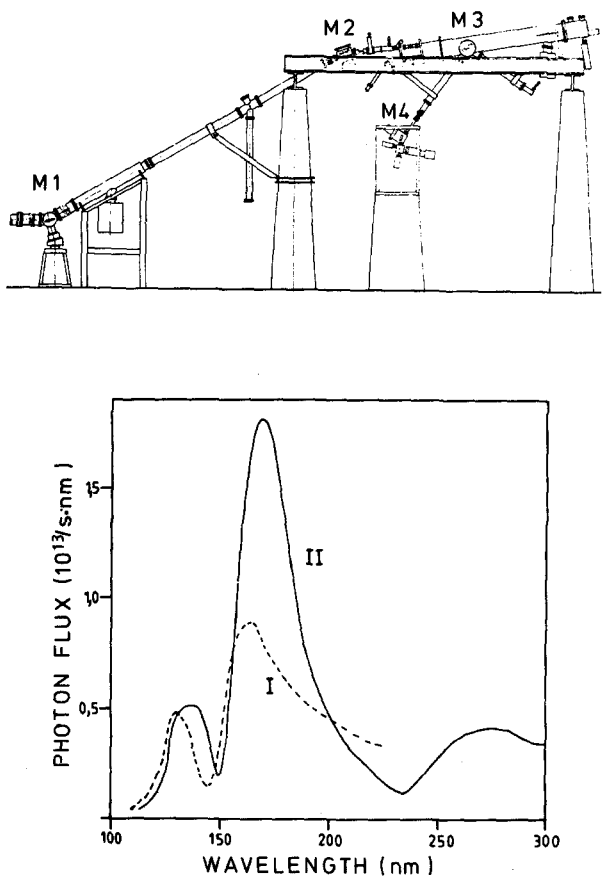

FIG. 1. Top: Scheme of the experimental set up with mirrors M1–M4. Bottom: Light flux at the sample for a BESSY current of 500 mA. (I) Holographic grating optimized for 100–300 nm. (II) Ruled grating blazed at 136 nm.

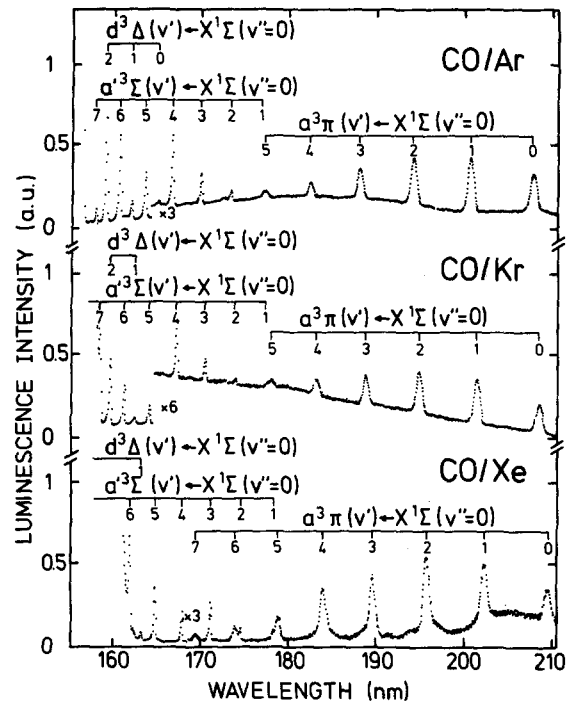

FIG. 2. Excitation spectra of the $a\,^3\Pi$, $a'\,^3\Sigma^+$, and $d\,^3\Delta$ vibrational progressions in Ar, Kr, and Xe matrices not corrected for the wavelength dependence of the incident light flux and taken for a strong Cameron emission band at 20 K.

for a contamination by for example N_2, O_2, or H_2O.

Lifting of the Pyrex cell[12] allows luminescence, transmission, and reflection experiments on a 5 mm thick doped crystal standing free in the ultrahigh vacuum chamber. Thick and optically clear samples are essential for the spectroscopy of triplet states of small molecules in matrices in order to obtain sufficient optical density for these very weak spin-forbidden transitions at concentrations low enough to prevent interaction between the dopants.

III. EXPERIMENTAL RESULTS

Transmission, excitation, and emission spectra have been taken for CO in Ar, Kr, and Xe matrices. Weak transitions show up in absorption spectra only as small dips on a large background of transmitted light. Details of such weak bands are displayed much better in excitation spectra in which the global fluorescence in zeroth order of the emission monochromator or the intensity in a strong emission band is recorded vs the wavelength of the exciting light. Excitation spectra are identical to absorption spectra for a state-independent quantum efficiency; otherwise the relative intensities of the bands would be modified. The transition energies and line shapes discussed in this paper are similar in transmission and excitation spectra and only the more pronounced excitation spectra will be presented. Figure 2 shows an overview of the excitation (absorption) spectra starting at low energies with the first triplet state $a\,^3\Pi(v')$ vibrational progression, continuing with the higher triplet states $a'\,^3\Sigma^+$, $d\,^3\Delta$, $e\,^3\Sigma^-$ and extending up to the first-allowed transition $A\,^1\Pi(v'=0)$. The spectra beyond and including

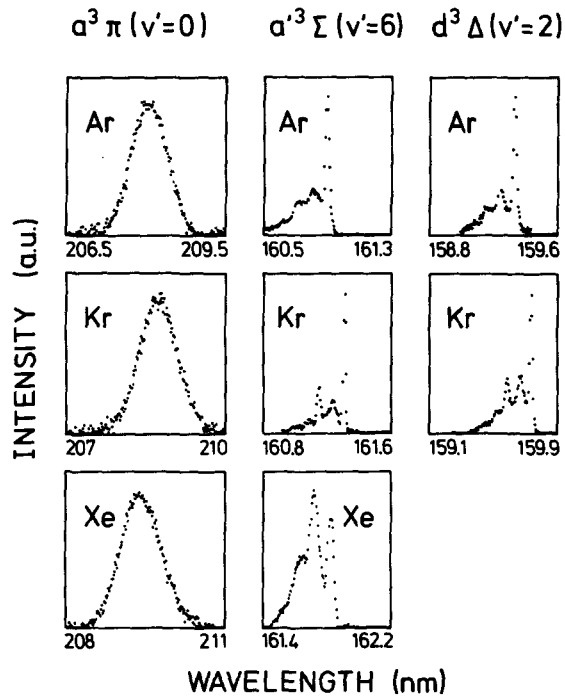

FIG. 3. Line shapes of several representative vibrational bands from Fig. 2 taken with a resolution of 0.013 nm at 8 K. The emission monochromator is used in zeroth order to increase the flux.

TABLE I. Wavelength (in nm) of absorption maxima in the $a\,^3\Pi$ bands and of the zero-phonon lines in the $a'\,^3\Sigma^+$, $d\,^3\Delta$, and $e\,^3\Sigma^-$ transitions. The fitted values (see the text) of ν_{00} (in eV), ω_e' (in meV), and $\omega_e'x_e'$ (in meV) are included.

					v'							
		ν_{00}	ω_e'	$\omega_e'x_e'$	0	1	2	3	4	5	6	7
$a\,^3\Pi$	gas	6.011	216.2	1.8	206.31			186.62	181.62	176.04	171.32	167.00
	Ar	5.957	218.5	2.2	208.14	200.93	194.37	188.24	182.76			
	Kr	5.938	218.7	2.7	208.83	201.57	195.02	188.99	183.40	178.36		
	Xe	5.921	214.6	1.8	209.43	202.23	195.62	189.49	183.90	178.69	173.86	
$a'\,^3\Sigma^+$	gas	6.864	152.2	1.3	180.63	176.77	173.14	169.72	166.48	163.42	160.52	157.77
	Ar	|6.852|[a]	149.0	1.0				170.16	166.93	163.87	160.95	158.20
	Kr	|6.834|	148.8	1.0				170.61	167.35	164.29	161.36	158.61
	Xe	|6.809|	150.0	1.1			174.57	171.12	167.86	164.77	161.87	
$d\,^3\Delta$	gas	7.517	144.8	1.2	164.84	161.77	158.86					
	Ar	|7.506|				162.23	159.38					
	Kr	|7.482|				162.70	159.78					
	Xe					163.19						
$e\,^3\Sigma^-$	gas	7.899	138.4	1.21	156.98	154.28	151.77					
	Ar	7.872			157.51	154.84						
	Kr	7.860			157.76	155.24						

[a] | | Extrapolated values.

$A\,^1\Pi(v'=0)$ are not shown because the oscillator strength of this dipole-allowed progression is about 10^6 times higher than that of the triplet states[7] and the bands are broadened by saturation. The strength of the singlet transitions has made them available in previous investigations.[2–5] The line shapes of representative members of the different triplet state progressions are collected in Fig. 3. The $a\,^3\Pi$ bands are significantly broader compared to the other triplet bands and they show a symmetric Gaussian profile with a FWHM of 24 meV which does not depend on the matrix. The structured $a\,^3\Sigma^+$, $d\,^3\Delta$, and $e\,^3\Sigma^-$ bands are composed of a zero-phonon line and phonon sidebands (Fig. 3). The widths of the zero-phonon lines in Ar and Kr matrices are limited by the experimental resolution. The wavelengths of the maxima in the $a'\,^3\Sigma^+$ bands and of the zero-phonon lines of the other progressions are collected in Table I together with the transition energies ν_{00}, the vibrational energies ω_e', and the anharmonicity parameters $\omega_e'x_e'$, fitted according to

$$\nu = \nu_{00} + (\omega_e' - \omega_e'x_e')v' - \omega_e'x_e'v'^2. \quad (1)$$

The width of the $a\,^3\Pi$ bands in absorption FWHM_A are contained in Table II and the gas-to-matrix shifts in absorption E_{GM} in Tables II and III. The energies of the phonon sidebands are listed in Table IV. Table IV demonstrates that the energies of the phonon sidebands in one matrix are very similar for the three electronic states $a'\,^3\Sigma^+$, $d\,^3\Delta$, and $e\,^3\Sigma^-$ but they differ in going from Ar to Kr and Xe matrices. The same holds also for the intensities of the sidebands relative to the zero-phonon lines, the widths and the shapes of the sidebands and the underlying backgrounds (Fig. 3). All these features are predominantly determined by the matrix for the a', d, and e transitions in contrast to the similarity of the $a\,^3\Pi$ absorption bands in the three matrices.

The dominant luminescence for a selective excitation of any one of the vibronic bands in Fig. 2 is shown in Fig. 4 and corresponds to the Cameron bands, $a\,^3\Pi(v'=0) \rightarrow X\,^1\Sigma_g^+(v'')$. The widths of the vibrational bands increases in going from Ar to Kr, and in Xe it is larger than the vibrational spacing, leading to a broad structureless hump. This hump already appears for the lowest $a\,^3\Pi(v'=0) \leftarrow X\,^1\Sigma_g^+(v''=0)$ excitation band in Fig. 2

TABLE II. Experimental lifetimes τ (in 10^{-3}s) gas-to-matrix shifts E_{GM}, Stokes' shifts, E_S, and linewidths, FWHM_A, (absorption) FWHM_E (emission) for the $a\,^3\Pi$ state. The relaxation energies $E_e = S_e\hbar\omega_g$, $E_g = S_g\hbar\omega_e$ and the phonon energies $\hbar\omega_e$,$\hbar\omega_g$ in the excited state e and ground state g, respectively, as well as the quadratic coupling strength B_e and the change in the configuration coordinate Δq^2 (in Å^2 amu) are deduced by a momentum analysis (see the text and Fig. 5). All energies in meV. τ for Ar from Ref. 7.

	Ar	Kr	Xe
τ	7.2	0.233	0.019
E_{GM}	54	73	90
E_s	44	250	1382
FWHM_A	24	24	24
FWHM_E	59	225	620
E_e	14	35	95
E_g	29	210	1278
$\hbar\omega_e$	10.5	7.2	4.0
$\hbar\omega_g$	15.5	17.8	14.8
B_e	− 0.513	− 0.833	− 0.927
Δq^2	1.062	5.552	48.961

TABLE III. Gas-to-matrix shifts E_{GM} (in meV) given by the differences of the ν_{00} values in the gas and in the matrix listed in Table I. E_{GM}^F are calculated shifts (see the text).

	Ar	Kr	Xe
$a\,^3\Pi$	54	73	90
$a'\,^3\Sigma^+$	12	30	55
$d\,^3\Delta$	11	35	...
$e\,^3\Sigma^-$	27	39	...
E_{GM}^F	64	50	73

TABLE IV. Energy separation of the first and second phonon-sideband from the zero-phonon line for the $a'\ ^3\Sigma^+$, $d\ ^3\Delta$, and $e\ ^3\Sigma^-$ transition. Librational energies $\hbar\omega_{lib}$ and local-phonon energies $\hbar\omega_{loc}$ for the electronic ground state of CO (Ref. 1) and the high energy cutoff $\hbar\omega_{max}$ of the lattice phonons (Ref. 27) are given for comparison. All energies in meV.

		Ar	Kr	Xe
$a'\ ^3\Sigma^+$	1	4.2	3.1	4.8
	2	8.1	7.3	8.5
$d\ ^3\Delta$	1	4.5	3.1	
	2	8.4	7.2	
$e\ ^3\Sigma^-$	1	4.1		
$\hbar\omega_{lib}$		1.8		
$\hbar\omega_{loc}$		9.97	8.47	6.5
$\hbar\omega_{max}$		8.06	6.16	5.25

and the intensity of this hump follows this excitation spectrum which supports our assignment of the hump to the Cameron bands. In addition, the lifetimes τ measured for this hump in Xe and for the well resolved Cameron bands in Kr and Ar, show a monotonic decrease with the atomic weight of the matrix (Table II) as is expected by the heavy atom effect.[7] Nevertheless the lifetimes are long, indicating a spin-forbidden triplet–singlet transition. The dashed high energetic wing seen in the spectrum in a Xe matrix is a contribution from the $A\ ^1\Pi(v'=0)\rightarrow X\ ^1\Sigma_g^+(v''=0)$ transition. This wing is missing for an excitation of the triplet states below $A\ ^1\Pi(v'=0)$, its intensity shows a maximum for excitation of $A\ ^1\Pi(v'=0)$ and the lifetime lies in the ns regime, as expected for a spin-allowed transition.

In Ar and Ne matrices, additional emissions at shorter wavelength due to other triplet states decaying to the ground state have been observed with some order of magnitude lower intensities. Several progressions in the ultraviolet and visible spectral region due to transitions between triplet states for excitation energies above $A\ ^1\Pi(v'=0)$ have been seen in Ne, Ar, and Kr matrices. All these additional emission bands will be treated in a forthcoming publication.

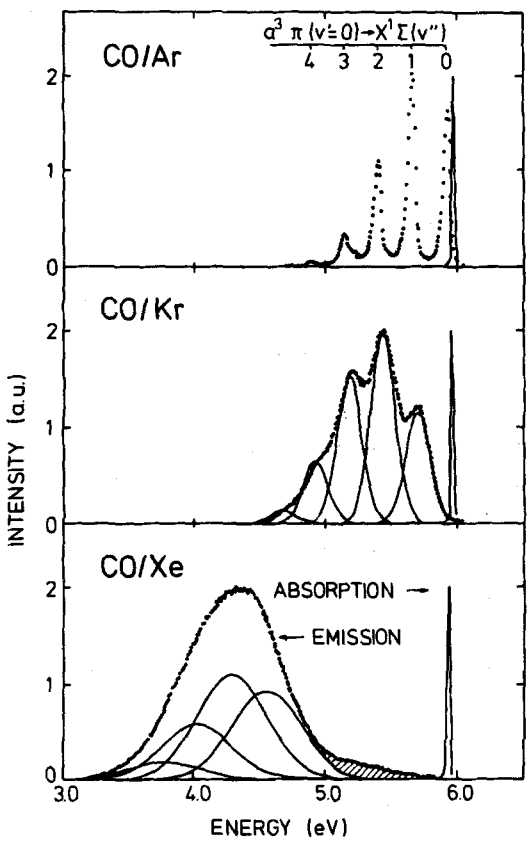

FIG. 4. Emission spectra (points) showing the Cameron bands and a deconvolution for the different vibrational members in Kr and Xe (solid lines) using Gaussian line shapes and gas-phase vibrational spacings. Intensities in the original experimental spectra taken on a linear wavelength scale have been multiplied by λ^{-2} to convert from a constant $d\lambda$ to a constant energy interval $d\nu$ and have been corrected for the sensitivity of the detection system. For Xe, the $A\ ^1\Pi(v'=2)$ state has been excited and the dashed wing is due to an $A\ ^1\Pi$ emission band (see the text). The narrow lines near 6 eV give for comparison the $a\ ^3\Pi(v'=0)\leftarrow X\ ^1\Sigma_g^+(v''=0)$ absorption bands.

IV. DISCUSSION OF THE $a\ ^3\Pi$ ABSORPTION AND EMISSION BANDS

The comparison of the $a\ ^3\Pi(v'=0)\leftrightarrow X\ ^1\Sigma_g^+(v''=0)$ transitions in absorption and emission in Fig. 4 illustrates that the Stokes shift E_S between the maxima of the bands increases by about a factor of 30 from 44 meV in an Ar matrix up to ~1.4 eV in a Xe matrix. The widths of the emission bands show a similar trend and the individual vibronic bands are no longer resolved in a Xe matrix. A fit with a Gaussian line shape and the gas phase vibrational spacings yields a deconvolution as shown in Fig. 4 for Kr and Xe matrices. The resulting Stokes shifts E_S and the linewidths in emission FWHM_E are also collected in Table II. The intensity disbtributions in the vibrational bands are similar to the gas phase Franck–Condon factors in an Ar matrix but higher v'' levels are more intense in a Kr matrix.

The origin of the Stokes shift and of the width of the bands is a structural rearrangement in the vicinity of an excited CO molecule caused by the different interaction of the $X\ ^1\Sigma_g^+$ ground state and the $a\ ^3\Pi$ excited state with the surrounding matrix atoms. Phonon sidebands are induced by this structural relaxation. The strength of these sidebands increases for larger changes of the nearest neighbor separations and is reconciled by a phonon coupling strength. Evidently the phonon coupling strength for the $a'\ ^3\Sigma$ and $d\ ^3\Delta$ transitions is moderate, leading to only few phonon sidebands with intensities similar to those of the zero-phonon lines (Fig. 3). For the $a\ ^3\Pi$ transition the coupling is strong, the zero-phonon lines are suppressed, and the intensity is shifted to multiphonon sidebands. The structures of individual sidebands are washed out due to a superposition of many bands with different phonon energies and perhaps some inhomogenous contributions. The spectra show only the envelope of the sidebands (Figs. 3 and 4) with a width given by the phonon sideband distributions, with maxima near the dominant phonon sidebands, and with a Stokes shift given by the energy of the dominant phonon sideband above the zero-phonon line in absorption plus the energy of the dominant sideband below the zero-phonon line in emission. A rough estimate for the Stokes shift of about 1 eV in a Xe matrix with a typical phonon energy of about 5 meV shows

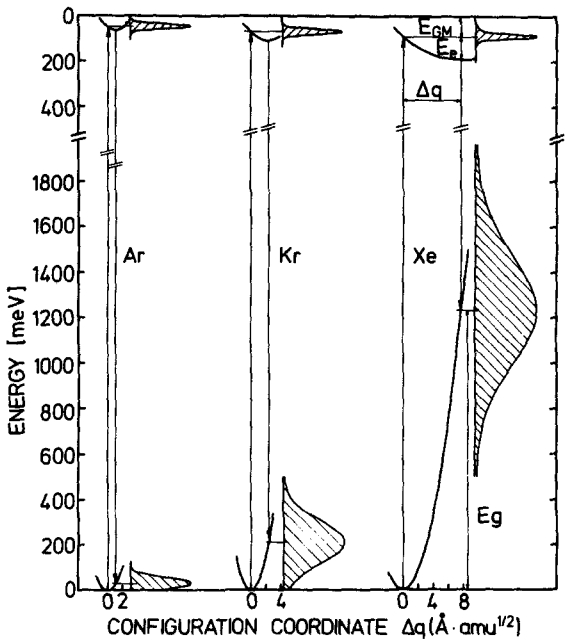

FIG. 5. Harmonic potentials for the $a\,^3\Pi$ state in Ar, Kr, and Xe matrices from the configuration coordinate analysis with ground-state relaxation energy E_g, excited state relaxation energy E_e, change in coordinate Δq, and gas-to-matrix shift E_{GM}. The upper and lower shaded bands are the absorption and emission bands, respectively. Δq corresponds to a shortening of the CO matrix separation.

that on an average about 200 phonons are created in an absorption–emission event due to the lattice relaxation. In general, a configuration coordinate model is used to relate the spectroscopic informations to the potential energy surfaces of the different electronic states of the dopant in the matrix. Analytic expressions have been worked out for the case of one dominant configuration coordinate q (for example, the nearest neighbor separation) in the harmonic approximation with one dominant phonon frequency $\hbar\omega_g$ in the ground state and one in the excited state $\hbar\omega_e$.[13,14] For linear coupling, which is the lowest level of approximation, the same phonon frequencies in the ground state and excited state are assumed ($\hbar\omega_g = \hbar\omega_e$) and only the minima of the parabola are displaced by Δq. Mirror images centered at the zero-phonon line are predicted for absorption and emission bands. A higher order of approximation is required to account for the much larger linewidths in emission compared to absorption (Fig. 4). The relevant parts of the excited state potential surface have to be significantly flatter than those of the ground state either due to anharmonicity or in the harmonic approximation due to $\hbar\omega_e < \hbar\omega_g$ (quadratic coupling). Quadratic coupling is preferred in the literature[15] and we use it together with the method of moments[16] to analyze the line shapes. M_1^A, M_1^E are related to the centers of the bands, M_2^A and M_2^E to the half-widths in absorption (A) and emission (E), respectively. S_e,S_g correspond to the displacement Δq (linear coupling strength), B_e,B_g to the difference in phonon frequencies ($\hbar\omega_e \neq \hbar\omega_g$, quadratic coupling strength) in the excited state (e) and ground state (g), respectively, and E_0 to the energy difference of the minima of the parabola. The four independent parameters E_0,

TABLE V. Shortening Δr of the separation between CO guest and closest matrix atoms in the $a\,^3\Pi$ state relative to the ground-state configuration. Δr_{cp} and Δr_{cs}: configuration coordinate model with effective mass of CO and one matrix atom or CO and a shell of 12 matrix atoms, respectively. Δr_{LJ}: from Lennard-Jones pair potential. Δr_{di} from dispersive and inductive interactions. $\epsilon(a\,^3\Pi)$, $\sigma(a\,^3\Pi)$: Lennard-Jones parameters for the $a\,^3\Pi$ state according to Ref. 17 and the text. All Δr values and σ values in Å, ϵ in meV.

	Ar	Kr	Xe
Δr_{cp}	0.25	0.51	1.45
Δr_{cs}	0.20	0.45	1.33
Δr_{LJ}	0.15	0.49	0.92
Δr_{di}	0.03	0.11	0.21
$\epsilon(a\,^3\Pi)$	18	25	50
$\sigma(a\,^3\Pi)$	3.14	3.07	2.62

S_e, $\hbar\omega_g$, $\hbar\omega_e$ necessary to describe the potential surfaces have been drived from the four available experimental moments M_1^A, M_1^E, M_2^A, M_2^E by the following relations which hold for $kT < \hbar\omega_g, \hbar\omega_e$:

$$M_1^A = E_0 + S_e\hbar\omega_g + B_e\hbar\omega_g/4, \tag{2}$$

$$M_1^E = E_0 - S_g\hbar\omega_e - B_g\hbar\omega_e/4, \tag{3}$$

$$M_2^A = S_e(\hbar\omega_e)^2, \tag{4}$$

$$M_2^E = S_g(\hbar\omega_g)^2. \tag{5}$$

The quadratic coupling terms, the displacements Δq and S_g are determined by the previous parameters:

$$S_e = \Delta q^2\omega_e^2/(2\hbar\omega_g), \tag{6}$$

$$S_g = \Delta q^2\omega_g^2/(2\hbar\omega_e), \tag{7}$$

$$B_e = (\omega_e^2 - \omega_g^2)/\omega_g^2, \tag{8}$$

$$B_g = (\omega_g^2 - \omega_e^2)/\omega_e^2. \tag{9}$$

The results of this analysis are given in Table II in terms of the relevant phonon energies $\hbar\omega_g$,$\hbar\omega_e$, of the relaxation energies $E_e = S_e\hbar\omega_g$, $E_g = S_g\hbar\omega_e$ in the excited state (absorption) and ground state (emission) potential surfaces, respectively (Fig. 5), the quadratic coupling strength B_e and the change in the configuration coordinate Δq. The ground state relaxation energies and phonon frequencies are significantly larger than those of the excited states, as is expected from the larger linewidth in emission. This asymmetry is also expressed by large quadratic coupling terms which are not too far from the limiting value of one. The relation between linewidth and relaxation energies and the strong increase in the relaxation energies in going from Ar to Xe is illustrated in Fig. 5. The relaxation energies are determined by the linear coupling terms; S_g is about 2 in an Ar matrix and increases up to 300 in a Xe matrix. The linear coupling terms are a measure of the displacement Δq of the equilibrium configuration coordinates in the ground and excited state. Δq is related to spatial rearrangements Δr by

$$\Delta r^2 = \Delta q^2/\mu \tag{10}$$

with a reduced mass μ of the particles. For a rough estimate we place CO in a substitutional site and we can assume that, for example, a symmetric structural relaxation of the 12 neighboring matrix atoms takes place. Δq corresponds in

this case mainly to a change of the radius of the shell of nearest neighbor atoms and the appropriate μ values lead to the Δr_{cs} values given in Table 5. Another extreme case would be a dominant assymetric change of the separation of CO and only one nearest neighbor matrix atom with the corresponding Δr_{cp} values listed also in Table II. The positive sign of the gas-to-matrix shift E_{GM} indicates an attractive interaction of CO in the a $^3\Pi$ state with the rare gas matrix which significantly increases from Ar to Xe. The subsequent structural relaxation leading to a further energy release by $S_e\hbar\omega_g$ is, therefore, due to a reduction in the CO matrix separation by an amount of the order of Δr_{cp} or Δr_{cs}. In summary, a rather consistent picture is obtained from the configuration model. The attractive interaction in the $a\ ^3\Pi$ state leads to smaller CO–matrix separations, flatter potential surfaces, and smaller phonon energies compared to the ground state. The radiative decay at the smaller equilibrium separation terminates at the strongly repulsive part of the ground state causing larger relaxation energies in the ground state and greater linewidths in emission. It is not surprising that all these features are more pronounced in the more polarizable Xe matrix than in Ar. The relaxation energies E_e and E_g are directly related to the spectroscopic data and are therefore reliable. The trends in the phonon energies concerning the differences between ground state and excited states and concerning the atomic weight of the matrix are expected to be correct but the numerical values are based on the harmonic approximation and have to be considered with caution. Δr is of the order of 1 Å and increases significantly from Ar to Xe but the numerical values rely on the interpretation of the configuration coordinate.

In an attempt to further substantiate the Δr values, we tried the model of Roncin[17] which rests on a lattice sum of Lennard-Jones pair potentials with the guest molecules in a substitutional site. The potential surfaces are described by matrix-dependent Lennard-Jones parameters σ, ϵ for the ground state and σ^*, ϵ^* for the $a\ ^3\Pi$ state. σ and ϵ are known from summation rules.[17] We calculated for each matrix the structural relaxation Δr_{LJ} from the ground state relaxation energy E_g. The model predicts the same trend and order of magnitude as the configuration coordinate model (Table V) but the Δr_{LJ} values are all somewhat smaller than the Δr_{cp} or Δr_{cs} values. σ^* and ϵ^* are derived from E_e and E_{GM}. The model is not really satisfying because a subtraction of the σ_M values of the matrix from σ^* yields $\sigma(a\ ^3\Pi)$ values dependent on the matrix (Table V) in contradiction to the basic assumptions of the model. The situation is even worse for the $\epsilon(a\ ^3\Pi)$ values (Table V).

Mohammed *et al.*[8] calculated from the lattice sums of dispersive and inductive interactions matrix shifts for the $a\ ^3\Pi$ transition in the ground state nuclear configuration, i.e., for absorption, again placing CO into a substitutional site. They compared these predictions with their luminescence energies[7] by assuming that the gas-to-matrix shift in absorption is equal to the gas-to-matrix shift in emission. The discrepancy by a factor of 7 for the Kr matrix led them to the conclusion that CO takes an interstitial site in the Kr matrix. The gas-to-matrix shift in emission consists of the gas-to-matrix shift in absorption E_{GM} (Table II) and the much larger Stokes shift E_s (Table II) which has been neglected in Ref. 8 because it was unknown. A comparison of the gas-to-matrix shift E^F_{GM} for the substitutional site (Table III) from Ref. 8 with the experimental shift in absorption E_{GM} shows an agreement within about 30% for all three matrices, Ar, Kr, and Xe. Therefore, this model is consistent with a substitutional site in all rare gas matrices. A better agreement cannot be expected because the gas-to-matrix shift for different electronic states should weakly and monotonically increase with the transition energy (E_1 in Ref. 8) according to this model. The experimental gas-to-matrix shifts of the higher-lying $a'\ ^3\Sigma^+$, $d\ ^3\Delta$, and $e\ ^3\Sigma^-$ states (Table III) are all smaller, in contradiction to the model, but lie within a range of 30% except for the Ar matrix, where discrepancies up to a factor of 4 occur. For improvement, a more detailed treatment of the attractive parts of the pair potential for different electronic states of CO and the inclusion of repulsive terms would be necessary.

Nevertheless, we have attempted a further estimate of the lattice relaxation Δr_{di} for the average distance between CO and the matrix atoms by using this model. The energy release ΔE in the $a\ ^3\Pi$ state by a lattice relaxation from the geometry R_u, R_v to R'_u, R'_v with $\Delta r_{di} = R_u + R_v - R'_u - R'_v$, according to Ref. 8, has been compared with the excited state relaxation energy E_e from the moment analysis (Table II). This yields a structural relaxation, Δr_{di}, listed in Table V.

The Δr_{di} values are significantly smaller than the structural relaxation predicted by the previous models. An underestimation of the structural relaxation by this model is not surprising because the neglect of repulsive terms in the potential leads to an unrealistic decrease of the energy by r^{-6}. Therefore, the results of the configuration coordinate model and of the Lennard-Jones pair potentials are more reliable.

Finally emission spectra of doubly-doped matrices with 0.1% CO, 3% Xe, 97% Ar, and 0.1% CO, 3% Xe, 97% Kr have been recorded to decide whether an asymmetric bonding between CO and one neighboring matrix atom or a symmetric relaxation of the whole first shell of matrix atoms is dominant. The spectra show a broad emission band with energy position and linewidth identical to that for CO in a pure Xe matrix together with emission bands similar to those for CO in pure Ar or pure Kr matrices, respectively. The probability that a CO guest molecule is surrounded by 1 Xe atom and 11 matrix atoms is high for the chosen concentrations. The relative intensities of the emission bands in one spectrum correspond to the probability for finding one Xe atom in the first shell around a CO molecule compared to the probability for finding no Xe atom—i.e., only Ar (or Kr) atoms—in the vicinity. The experiment shows that one neighboring Xe atom in the doubly-doped samples is sufficient to induce the same Stokes shift and linewidth in emission as for 12 surrounding Xe atoms in a pure Xe matrix. The dominant structural relaxation in a Xe matrix is a displacement of CO to one neighboring Xe atom and the formation of a strongly bound pair with a bond length reduced by 1.5 Å compared to the ground state. This asymmetric relaxation with a movement of the CO molecule justifies the use of the pair effective mass in Eq. (10).

V. PHONON SIDE BANDS OF THE $a'\,^3\Sigma^+$ AND $d\,^3\Delta$ STATES

The higher triplet states $a'\,^3\Sigma^+$, $d\,^3\Delta$, and $e\,^3\Sigma^-$ show sharp zero-phonon lines and some phonon sidebands of moderate intensities (Fig. 3), in strong contrast to the broad multiphonon bands of the $a\,^3\Pi$ state. Evidently, the transitions to higher triplet states couple weakly to the lattice with Huang–Rhys coupling constants S which are smaller than 0.5 in Ar and Kr matrices and of the order of one in Xe matrices. The significantly higher coupling constant of the $a\,^3\Pi$ transition in all matrices suggests that the coupling is determined by the symmetry of the electronic wave functions involved. A transition from the spherical symmetric Σ ground state to the asymmetric Π state initiates a strong and perhaps anisotropic lattice relaxation and a strong coupling. The lattice relaxations, and thus couplings, due to transitions to the spherical symmetric $a'\,^3\Sigma^+$, $e\,^3\Sigma^-$ states and the rather highly symmetric $d\,^3\Delta$ state are weak. An identification of the phonon modes contributing to the sidebands is complicated by the fact that the lattice of the host is distorted by the guest and local modes, and librations can be involved in addition to lattice modes. Furthermore, the energies of the local phonon modes and the librations are determined by the guest–host potential surfaces which are different in the electronic ground state of the molecule and in excited states, as has been shown before for the $a\,^3\Pi$ state. Experimental investigations or calculations of the phonon modes in the excited states are not available. Theoretical results and data from infrared absorption experiments related to the ground state will be used as guidelines.

Two sidebands are identified for the a' and d states, one centered in the region of 3–5 meV and one centered around 7–8.5 meV in the different matrices (Table IV). If the two bands are due to a progression in a single mode, then the spacings between the first and second bands should be equal to or perhaps smaller (anharmonicity) than the energy of the first mode. The spacings of 4.2 and 4.1 meV between the first and second band of the a' and d states in a Kr matrix are significantly larger than the energy, 3.1 meV, of the first mode and, therefore, the two bands represent different modes. The analogy in the energies suggests that the bands correspond to two independent modes in Ar and Xe matrices also.

The high-energy mode lies beyond the high-energy cutoff $\hbar\omega_{\max}$ of the lattice phonon modes in all three matrices (Table IV). It has to be attributed to a local mode induced by the CO guest. The energies of this mode are in the region of the calculated[1] and observed ($\hbar\omega_{\rm loc}$) local modes in the electronic ground state (Table IV). The trend to lower energies in going from Ar to Xe is not reproduced in the excited state.

The low-energy mode is also not related in a convincing way to a density of states in the lattice phonon modes. Therefore, it is likely to involve low-energy local modes and those of lowest energy are librations. The librational energy in the ground state in an Ar matrix for a transition of $n = 0$ to $n = 1$ is 1.8 meV (Table IV). The normalized transition energy E/B increases with K/B in the Devonshire model.[18] K represents the barrier height hindering the rotation and B is the rotational constant. Including the decrease in B to $\tilde{B}$ due to the pseudorotating matrix cage[19] yields $\tilde{B} = 0.15$ meV and $K = 2$ meV for the libron in the electronic ground state of CO in the Ar matrix. $\tilde{B}$ will somewhat decrease in the excited electronic states because of the smaller B values. Therefore, librational energies of 3–4 meV will correspond to K/B values of 40 to 60 and barrier heights of the order of 6 meV. An increase of the barrier height in the excited states is not surprising in view of the stronger interaction of the molecule with the matrix, which is evident, for example, from the gas-to-matrix shift.

The spectroscopic data presented in this paper form a basis for the investigation of radiative and nonradiative relaxation processes in the excited electronic and vibrational states of CO molecules in matrices. Studies similar to those already performed for N_2[20] are in progress.

ACKNOWLEDGMENTS

The strong experimental support of U. Fischer and the backing of the BESSY crew in the installation of the beam line is gratefully acknowledged. We thank Professor A. Tramer for suggesting to us experiments on doubly-doped matrices. This work has been financially supported by the Bundesministerium für Forschung und Technologie by Contracts No. 244SW and 313AXC3-11.

[1] H. Dubost, Chem. Phys. **12**, 139 (1976).
[2] P. Gürtler, Thesis, Hamburg, 1979, and internal report DESY F41-79/06.
[3] E. Boursey and V. Chandrasekharan, *International Conference on Vacuum Ultraviolet Radiation Physics*, edited by M. C. Castex, M. Pouey, and N. Pouey (Montpellier, 1977), Vol. 1, p. 67.
[4] J. Y. Roncin, J. Mol. Spectrosc. **26**, 105 (1968); J. Y. Roncin, N. Damany, and J. Romand, *ibid.* **22**, 154 (1967).
[5] I. Ya Fugol, L. I. Timchenko, Yu. B. Poltoratskiĭ, and A. G. Belov, Izv. Akad. Nauk SSSR Ser. Fiz. (Bull. Acad. USSR Phys. Ser.) **40**, 471 (1978).
[6] K. J. Swyler, Thesis, 1973.
[7] J. Fournier, H. H. Mohammed, J. Deson, and C. Vermeil, J. Chem. Phys. **73**, 6039 (1980).
[8] H. H. Mohammed, A. M. Taleb, and J. Fournier, Chem. Phys. **91**, 267 (1984).
[9] H. Wilcke, W. Böhmer, and N. Schwentner, Nucl. Instrum. and Methods **204**, 533 (1983).
[10] J. Bahrdt, and N. Schwentner, Nucl. Instrum. Methods **216**, 237 (1983).
[11] I. Munro and N. Schwentner, Nucl. Instrum. Methods **208**, 819 (1983).
[12] W. Rudnick, R. Haensel, H. Nahme, and N. Schwentner, Phys. Status Solidi **87**, 319 (1985).
[13] C. M. Lax, J. Chem. Phys. **20**, 1752 (1952). R. C. O'Rourke, Phys. Rev. **81**, 265 (1953). T. H. Keil, Phys. Rev. A **140**, 601 (1965).
[14] C. M. Weinert, F. Forstmann, H. Abe, R. Grinter, and D. M. Kolb, J. Chem. Phys. **77**, 3392 (1982).
[15] For example, see D. Hsu and J. L. Skinner, J. Chem. Phys. **83**, 2107 (1985).
[16] In Ref. 14, the second term of Eq. (4a) should contain $\hbar\omega_g(j)$ instead of $\hbar\omega_e(j)$ and the sign of B_e, B_g is consistent with Ref. 15.
[17] J. -Y. Roncin, Chem. Phys. Lett. **3**, 408 (1969).
[18] A. F. Devonshire, Proc. R. Soc. London Ser. A **153**, 601 (1936).
[19] J. Manz and K. Kirsky, Chem. Phys. **46**, 457 (1980).
[20] H. Kühle, J. Bahrdt, R. Fröhling, N. Schwentner, and H. Wilcke, Phys. Rev. B **31**, 4854 (1985). H. Kühle, R. Fröhling, J. Bahrdt, and N. Schwentner, J. Chem. Phys. **84**, 666 (1986).
[21] H. Bilz and W. Kress, in *Phonon Dispersion Relations in Insulators* (Springer, Berlin, 1979); B. M. Powell and G. Dolling, in *Rare Gas Solids*, edited by M. L. Klein and J. A. Venables (Academic, London, 1977), Vol. II.